SANDIA REPORT SAND83—1909 • Unlimited Release • UC—60
Printed September 1984

Modeling Stochastic Wind Loads on Vertical Axis Wind Turbines

Paul S. Veers

Prepared by
Sandia National Laboratories
Albuquerque, New Mexico 87185 and Livermore, California 94550
for the United States Department of Energy
under Contract DE-AC04-76DP00789

Issued by Sandia National Laboratories, operated for the United States Department of Energy by Sandia Corporation.

Printed in the United States of America
Available from
National Technical Information Service
U.S. Department of Commerce
5285 Port Royal Road
Springfield, VA 22161

NTIS price codes
Printed copy: A19
Microfiche copy: A01

MODELING STOCHASTIC WIND LOADS ON VERTICAL AXIS WIND TURBINES

Paul S. Veers

Applied Mechanics Division 1524
Sandia National Laboratories
Albuquerque, New Mexico

Abstract

The Vertical Axis Wind Turbine (VAWT) is a machine which extracts energy from the wind. Since random turbulence is always present, the effect of this turbulence on the wind turbine fatigue life must be evaluated. This problem is approached by numerically simulating the turbulence and calculating, in the time domain, the aerodynamic loads on the turbine blades. These loads are reduced to the form of power and cross spectral densities which can be used in standard linear structural analysis codes. The relative importance of the turbulence on blade loads is determined.

Introduction

The most common design for Vertical Axis Wind Turbines (VAWT's) was first patented in 1931 by Darrieus, a Frenchman. This "egg beater" shaped machine consists of one or more blades with airfoil cross sections attached to the top and bottom of a central shaft, or tower. To minimize bending stresses in the blades while the turbine rotates, the blades usually have a characteristic troposkien, or "spinning rope," shape. Torque is produced when the turbine rotor turns in the wind. Fig. 1 shows the 17 meter research VAWT at Sandia National Laboratories, Albuquerque, NM. This turbine has the most common configuration of VAWT's currently being built; two blades with a central tower and guy cables supporting the top of the rotor.

The aerodynamic analysis of the VAWT is complicated by several factors. Since the VAWT blade rotates through 360 degrees relative to the incident wind during each rotation, the rate of change of angle of attack is often much greater than experienced in other airfoil applications. But because the speed of the blade is normally much greater than the wind speed, the angle of attack varies between positive and negative values around zero degrees. The higher the wind speed, the greater the angle of attack excursions. When the winds become high enough, the angles of attack become large enough that the airfoil begins to stall dynamically. Research in VAWT aerodynamics is currently investigating both dynamic stall and pitch rate effects. Aerodynamic analysis using the streamtube momentum balance approach was the earliest and simplest approach used to estimate VAWT performance[1]. The vortex lifting line approach has produced some better results, in an average sense, over a wider range of wind conditions[2], but is computationally expensive. Both methods suffer from the lack of a validated method of predicting dynamic stall. Except for empirical lift and drag curves from wind tunnel testing, accurate pitching airfoil, dynamic stall models do not exist. Most VAWT's experience stall over a significant portion of the normal operating range. The loss of lift due to stall in high winds is considered beneficial because it limits the maximum power that the drive train must transmit, thereby holding down the turbine cost.

The structural analysis of the VAWT must deal with the fact that the structure is rotating. Coriolis and centrifugal effects make the modes of vibration complex, but the system remains linear. Free vibration analysis and aeroelastic analysis are well developed and validated[3]. The forced vibration analysis of the VAWT rotor is developed; but agreement with field data from operating turbines is sometimes poor, especially in the high wind speed, significant stall, regime[4]. It is not yet clear whether the source of error is in the structural analysis or in the calculation of the aerodynamic loads. The relatively good agreement of the structural analysis to the data gathered at low wind speeds would seem to indicate that the problem may lie in the aerodynamics.

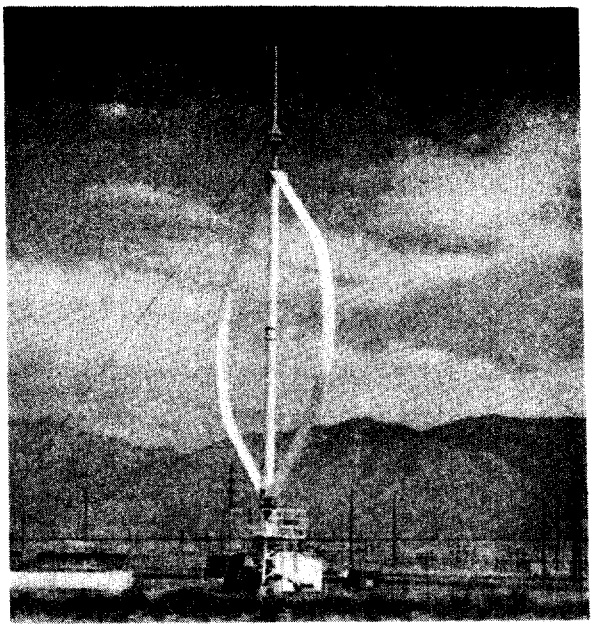

Fig. 1 Darrieus Vertical Axis Wind Turbine (VAWT) at Sandia National Laboratories, Albuquerque, NM.

Another possible source of error in previous load calculations is the assumption of a steady wind. Until now, all the aerodynamic loads have been calculated based on a constant ambient wind. The loads which result from this calculation are shown in Fig. 2. Tangential forces are defined as the component in the direction tangent to the path of the blade as it rotates and normal forces are normal to this path. The tangential forces produce a net torque about the central tower while the normal forces produce no net energy. When a constant wind is assumed, the forces repeat exactly for each rotor revolution. The frequency content of these forces is therefore limited to integer multiples of the turbine rotational speed (abbreviated as "per rev" frequencies). This approach will produce zero excitation at any frequency other than the per rev frequencies. This is not totally unreasonable because the per rev frequency content of the loads is produced by the mean wind and the rotation of the rotor, and is therefore large compared to the turbulence induced, stochastic loads. However, data collected from VAWT's operating in high winds have shown significant response at the structural resonant frequencies as well as at the per rev frequencies. The spectral content of the blade stress response shown in Fig. 3 could never be predicted with loads calculated assuming a steady wind.

By calculating the aerodynamic loads due to a turbulent wind, the loads will contain all frequencies, not only the per rev frequencies. These stochastic loads are described by their power spectral densities (psd's) and cross spectral densities (csd's). Because the relationship between incident wind speed and blade forces is

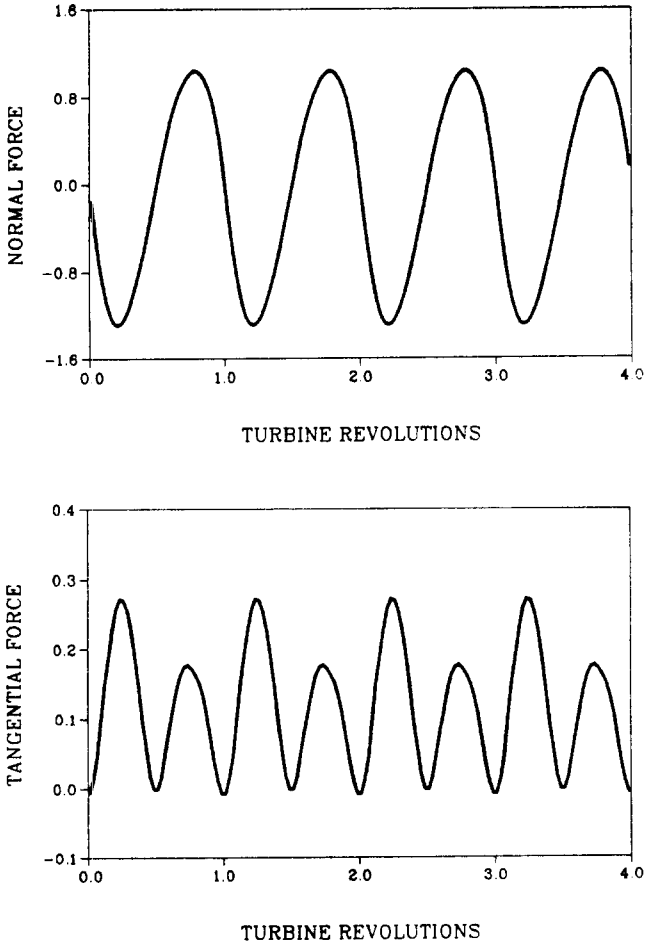

Fig. 2 Dimensionless Blade Loads calculated assuming a steady wind; (a) normal to the blade path, (b) tangential to the blade path.

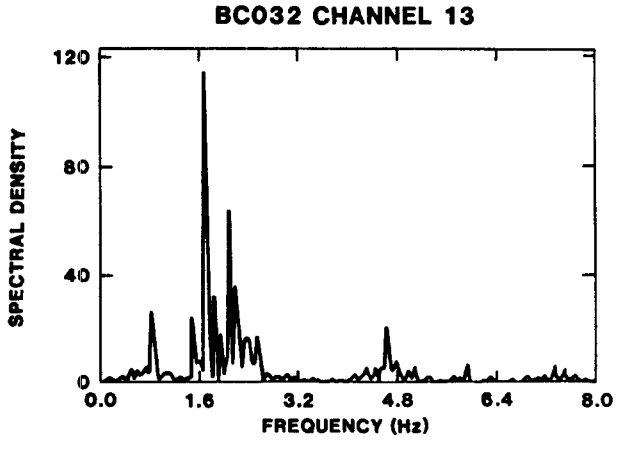

Fig. 3 Power spectral density (psd) of the stress in a VAWT blade measured during operation in high winds. The turbine rotational frequency is 0.8 Hz.

nonlinear, even before the onset of stall, the blade loads are calculated in a time marching manner. But since the structural response to the stochastic loads is linear, the psd's and csd's will be sufficient input for structural analysis.

Turbulent Wind Model

The first step in a time domain calculation of the the stochastic blade loads is to produce a numerical model of the atmospheric turbulence. The turbulence model must posses frequencies of interest for structural analysis (0 - 10 per rev). In a NASA summary of atmospheric environments by Frost, Long and Turner[5], the following form for the psd of atmospheric turbulence is suggested;

$$S(\omega) = \frac{c_1 \bar{V} h [\ln(10/z_o + 1)\ln(h/z_o + 1)]^{-1}}{1 + c_2[h\omega \ln(10/z_o + 1)/\bar{V} \ln(h/z_o + 1)]^{5/3}} \quad (1)$$

where

ω = frequency

h = height above ground

$\bar{V}$ = mean wind speed at h = 10m

z_o = surface roughness coefficient

c_1 and c_2 are constants which differ for each spatial component of turbulence. These constants are given as;

$c_{1x} = 12.3$; $c_{2x} = 192.$ for the longitudinal direction,

$c_{1y} = 4.0$; $c_{2y} = 70.$ for the lateral direction and

$c_{1z} = 0.5$; $c_{2z} = 8.0$ for the vertical direction.

An example turbulence psd at a reference height of 30ft (10m) with a surface roughness coefficient of .1 is shown in Fig. 4. For the wind velocity a

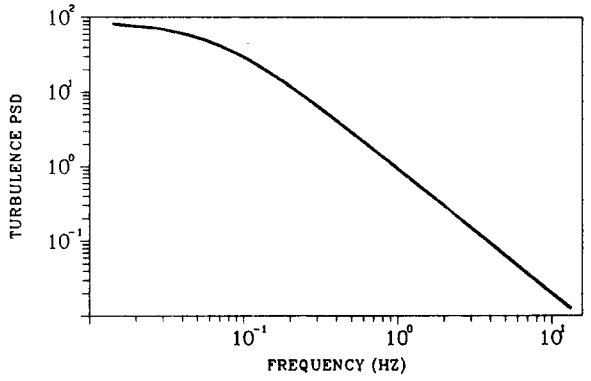

Fig. 4 Psd of turbulence using Eq. (1); h = 10m, Z_o = 0.1, $\bar{V}$ = 15 m/s.

Gaussian time series described by this psd can be obtained by the following method[6]. Represent the power in a narrow band, $\Delta\omega$, of the psd by sine and cosine components, with random phase, at the central frequency and sum these inputs over all the frequencies of interest. Such a velocity time history is given by,

$$V(t) = \bar{V} + \sum_{j=1}^{n} (A_j \sin\omega_j t + B_j \cos\omega_j t) \qquad (2)$$

where

$$A_j = \sqrt{\frac{1}{2} S_j \Delta\omega} \sin\phi_j$$

$$B_j = \sqrt{\frac{1}{2} S_j \Delta\omega} \cos\phi_j$$

S_j = magnitude of the psd at frequency ω_j

ϕ_j = a uniformly distributed random variable on the interval zero to 2π.

The central limit theorem guarantees convergence of V(t) to a Gaussian form as the number of sinusoidal components at different frequencies with random phase becomes large. This is equivalent to band limited, filtered white noise. If the frequency spacing is regular and begins at zero, the computation of the time series can be accomplished with a discrete inverse Fourier transform $\mathcal{F}^{-1}$ of the complex series,

$$V(t) = \bar{V} + \mathcal{F}^{-1} \sum_{j=1}^{n} (A_j + iB_j). \qquad (3)$$

If the three directional components of the turbulence are assumed to be uncorrelated, each component can be independently generated using the above method. The usual approach to transforming this temporal representation into a spatial variation is to use Taylor's frozen turbulence hypothesis. Using this approach, it is assumed that all turbulence is propagated in the longitudinal direction at the mean wind speed.

Fig. 5 shows a single point wind simulation time series where the horizontal longitudinal, and lateral velocity components have been resolved into magnitude and direction.

A simple approach to simulating a full three dimensional field of wind is to assume that the wind speed and direction in a plane normal to the mean wind direction are constant. This is obviously quite crude, but can be adequate if the region of interest in this plane is relatively small and the wind is highly correlated over that region. Frost[5] has an estimate of spatial coherence of the form,

$$\gamma_{ij}^2 = \exp(-a\ \omega\ \Delta r/\bar{V}) \qquad (4)$$

where

a = decay coefficient

ω = frequency

Δr = distance between points i and j

$\bar{V}$ = mean wind speed.

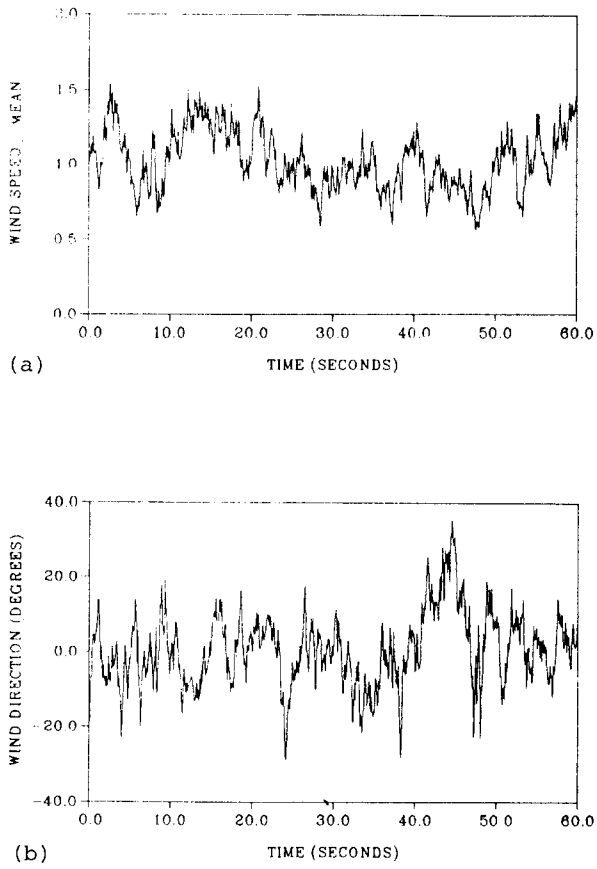

Fig. 5 Example simulated, single point, wind velocity time series, (a) wind speed, (b) wind direction.

The suggested value for the decay coefficient, "a," is 7.5 for both lateral and vertical separations. This expression indicates that the size of the region of significant correlation is a function of frequency and mean wind speed. For the 17m diameter VAWT's, the most common built to date, the coherence over the range of most energetic frequencies is greater than .5. This implies that the correlation over most of the swept area of the turbine rotor is quite high. For the larger rotors of the future, or the current large diameter propeller type turbines, the one dimensional wind variation may not be adequate.

A fully three-dimensional spatially varying wind can be simulated by producing time series of the wind speed at several points which lie in a plane perpendicular to the mean wind direction, as shown schematically in Fig. 6. The longitudinal variations are, as before, produced by Taylor's frozen turbulence hypotheses. The velocity time history at a particular point is reproduced at a downstream point at a later time. The time shift is equal to the distance between the points divided by the mean wind speed. The wind time series at each point is a random process which is correlated to wind at every other point. As shown by Eq. 4, the level of correlation depends on the distance between the points, the mean wind speed and its frequency.

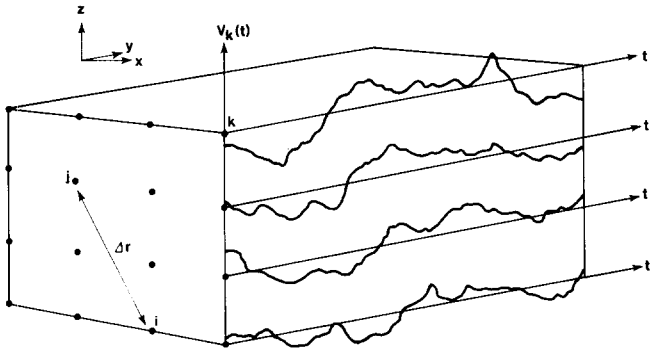

Fig. 6 Schematic of a wind simulation with variations in three dimensions. Correlated single point time series are generated at several input points.

Since the wind speed at each point can be represented by Gaussian random processes, the total input wind field can be represented as a random process vector, $\{V\}$. The second order statistics of $\{V\}$ can be defined by the spectral matrix $[S]$. The element in the i-th row and j-th column of $[S]$ is the cross spectral density (csd) between the wind speeds at input points i and j. The diagonal terms are the psd's of the input wind speeds. The csd's are related to the coherence function and the psd's by the expression,

$$\left|S_{ij}\right|^2 = \gamma_{ij}^2 \, S_{ii} \, S_{jj} \qquad (5)$$

where

γ_{ij}^2 = coherence function

S_{ij} = csd between points i and j

S_{ii} = psd at point i.

The csd's are, in general, complex functions of frequency. Eq. 5 relates only the magnitude of the csd's to the coherence and the psd's and is therefore insufficient to completely define the spectral matrix. Analytical expressions for the csd's have been suggested by Frost, but they are very complicated functions involving modified Bessel functions of fractional order. If the csd's are approximated as real functions, Eqs. 1, 4 and 5 can be used to define the spectral matrix. Since there is usually no relative phase between the winds at two points that are at the same height above the ground, the csd between these points is real. For points with some vertical separation, there is a tendency for the winds at the higher elevation to lead the lower elevation winds, which results in a complex csd. However, this tendency is not strong and the magnitude of the imaginary part is usually much smaller than the real part. The csd's are therefore assumed to be entirely real and approximated by Eq. 5.

The method of converting the spectral matrix into a vector of time series realizations of the random process follows[7]. Define a lower triangular matrix of transfer functions, $[H]$, such that

$$[H]^*[H]^T = [S] \qquad (6)$$

Physically, $[H]$ is a transfer matrix from uncorrelated white noise to the correlated spectra of the wind at the input points. In general, both $[S]$ and $[H]$ are complex, but for the degenerate case of a real $[S]$, $[H]$ is real also. The general case of a complex $[S]$ is derived in Ref. 7. Because $[H]$ is lower triangular, it is completely defined by Eq. 6. The elements of $[H]$ can be determined recursively:

$$\begin{aligned}
H_{11} &= S_{11}^{1/2} \\
H_{21} &= S_{21}/H_{11} \\
H_{22} &= (S_{22} - H_{21}^2)^{1/2} \\
H_{31} &= S_{31}/H_{11} \\
H_{32} &= (S_{32} - H_{31}\, H_{21})/H_{22} \\
&\vdots \\
H_{ii} &= \left(S_{ii} - \sum_{j=1}^{i-1} H_{ij}^2\right)^{1/2} \\
H_{ij} &= \left(S_{ij} - \sum_{k=1}^{j-1} H_{ik}\, H_{jk}\right)/H_{jj}
\end{aligned} \qquad (7)$$

Define $[X]$ as a diagonal matrix of complex frequency domain representations of independent white noise Gaussian signals with unit variance. The

correlated vector of wind random processes can then be calculated from

$$\{V\} = \mathcal{F}^{-1}([H][X])\{1\} \qquad (8)$$

where $\{1\}$ is a column vector of ones.

Multiplying [H] by [X] gives a random phase at each frequency to each column of [H]. The multiplication in (8) by the vector of ones has the effect of summing the rows of the inverse Fourier transform of [H][X]. Once [H] has been calculated, new unique realizations of the process can be formed simply by introducing a new [X] into Eq. 8.

The vector of wind turbulence components, $\{V\}$, has zero mean and describes only the turbulent part of the wind. The mean wind, which may vary with height to include wind shear effects, is added to the turbulent part.

The main difficulty in implementing this procedure is the size of the matrices involved. For N input points, the matrices [S], [H] and [X] are NxN. Each element in the matrices is a function of frequency which must be defined at each discrete input frequency. If the number of input points and discrete frequencies is not kept to a minimum, the size of the problem can easily exceed the core storage space on a main frame computer. In spite of the size of the problem, the use of the fast Fourier transform makes the computation relatively fast. Example problems which would exceed the core storage on a Cray were run on a VAX 11/780 in a few minutes.

In summary, a full field of turbulent wind can be simulated with variations in one to three spatial directions. The one dimensional variations are produced by creating a wind time series at a point and assuming that the wind speed is constant in a plane perpendicular to the mean wind direction. The longitudinal variation is achieved by applying Taylor's frozen turbulence hypothesis. A three dimensional wind field can be simulated by producing an array of correlated single point time series. The need for the three dimensional representation depends on the size of the wind field of interest. Larger fields have lower spatial correlation and require a multidimensional turbulence model. If the different components of the turbulence are uncorrelated, they can each be created independently by repeating the procedures outlined above.

The main difference between this turbulence simulation and other methods currently being developed (Ref. 8, 9, 10) is that in this simulation the turbulence is based solely on its first and second order statistical moments without any reference to the fluid dynamics of the wind. There is no guarantee that this simulated flow field will be continuous, compatible or physically realizable. However, by matching its first two statistical moments, the turbulence properties which have the most significant impact on the blade loads and therefore the structural response of the wind turbine are accurately represented. The risk of misrepresenting physical flow properties is balanced by the statistical accuracy and simplicity of this approach.

Aerodynamic Model

Various approaches to calculating the aerodynamic forces on a VAWT blade have been developed in the past. The earliest, and simplest, involves streamtube momentum balance methods[1]. Since then, vortex lifting line codes have been written which are more accurate over a wider range of operating wind speeds[2]. The cost of this generality is a tremendous increase in computational time needed to calculate the blade loads. A random blade load simulation necessitates a computationally fast method of converting instantaneous winds into blade loads. To reduce the statistical error, the loads must be calculated repeatedly and the psd and csd estimates averaged. The streamtube momentum balance method is by far the fastest available. Subdividing the swept area of the turbine rotor into a bundle of streamtubes creates a ready made computational grid. Each streamtube can be used as a location to input correlated single point wind speed time series. The wind speed at each point in the streamtube can then be tracked as it passes through the rotor.

The basic aerodynamic model used for this analysis was developed by Strickland. The method, which is comprehensively described in Ref. 11, will be outlined briefly here. The idea is to subdivide the rotor into streamtubes along the mean wind direction. As a blade passes through a streamtube, the flow is retarded. The amount of retardation is related to an "interference factor." The retardation is related to the net streamwise force by conservation of momentum within the streamtube. Because of the interdependence of streamwise force and angle of attack, the force calculation is iterative. Once the iteration converges, the angle of attack is found and the coefficients of normal and tangential force are interpolated from a table of values. The code used in this study neglects both Reynolds number and dynamic stall effects. The results reported here are for low wind speeds where these effects are relatively small.

Fig. 7 shows a typical streamtube as it passes through a VAWT rotor. As shown in the plan view, each streamtube is divided into three regions by intersections with the blade path: upstream, inside the rotor and downstream. The wind speed is reduced in each region by successive blade passages. Each streamtube has three mean wind speeds which correspond to the three regions. The mean wind speed inside the rotor, $\bar{V}_r$, is reduced from the mean free stream velocity, $\bar{V}_\infty$, by the interference factor which is calculated by assuming a steady wind. Although they propagate at the reduced mean wind speed, $\bar{V}_r$, the turbulence components transverse to the mean wind direction are assumed undiminished as they pass through the rotor.

The instantaneous wind speed at a given blade element is determined in the following manner:

For each streamtube, the winds which have passed through the plane just upwind of the rotor (see Fig. 7) in the recent past are stored. The length of time, Δt, required to traverse the distance from the upwind plane to the current position of the blade element is calculated by,

$$\Delta t = a/\bar{V}_\infty + b/\bar{V}_r \qquad (9)$$

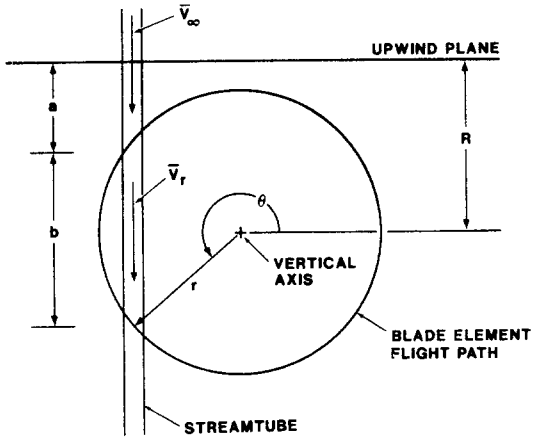

PLAN VIEW

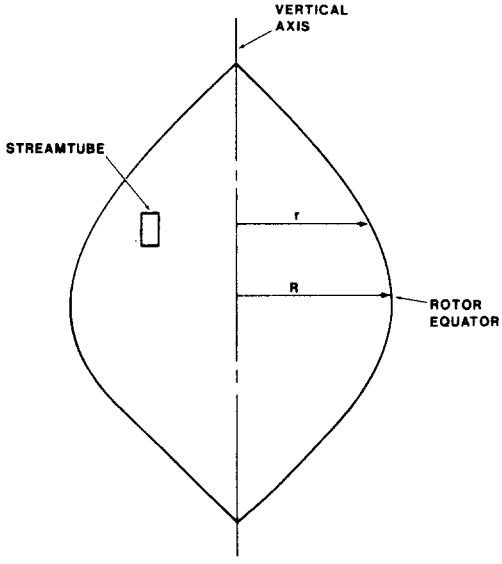

DOWNSTREAM VIEW

Fig. 7 The path of a typical streamtube with respect to the VAWT rotor. The mean freestream wind speed, $\bar{V}_\infty$, is reduced to $\bar{V}_r$ by the first blade passage and reduced again by the second blade passage.

where

$$a = R - |r \sin\theta| \qquad 0 < \theta < 2\pi$$

$$b = \begin{cases} 0 & 0 < \theta < \pi \\ |2r \sin\theta| & \pi < \theta < 2\pi \end{cases}$$

The wind speed that passed through the upwind plane at a time, Δt, earlier is then determined. For the downstream passage of the blade through the streamtube, the upwind wind speed is reduced by twice the mean upwind streamtube interference factor. An instantaneous interference factor and angle of attack are calculated and the instantaneous forces on the blade are determined.

Results and Discussion

If a steady wind is assumed, the calculated forces on the blade are identical for each rotation. Plots of the normal and tangential dimensionless forces near the turbine equator in a steady wind are shown in Fig. 2. The force components are defined in a reference frame fixed to the VAWT blade. The normal force changes direction as the blade passes through upwind and downwind orientations. The tangential force is almost always positive, only going to zero, or slightly negative, when the blade chord is aligned with the wind. The steady wind loads consist entirely of frequencies which are integer multiples of the turbine rotating frequency (per rev frequencies). Table 1 contains the sine and cosine coefficients of a Fourier series representation of these steady wind loads for a 50 ft (15m) diameter turbine in a 21 mph wind.

TABLE 1

PER REV FREQ.	NORMAL		TANGENTIAL	
	COS	SIN	COS	SIN
1	-2.21	18.8	-.001	-.926
2	1.37	2.15	-1.58	-.342
3	.216	1.32	-.043	.261
4	-.036	.302	-.192	-.063
5	-.073	.148	-.008	.014

Table 1 Cosine and sine coefficients of a Fourier series representation of the VAWT loads calculated assuming a steady wind. ($\bar{V}$ = 21 mph).

Fig. 8 shows plots of the normal and tangential components of the blade forces. These are the force components at the turbine equator calculated using a one dimensional turbulent wind simulation. The basic form of the steady loads is retained, but a stochastic component caused by the turbulence has been added to the underlying deterministic part. However, due to the nonlinear relationship between the incident wind and blade loads, this is not simply a superposition of the loads due to the steady wind and the loads due to the turbulent component of the wind.

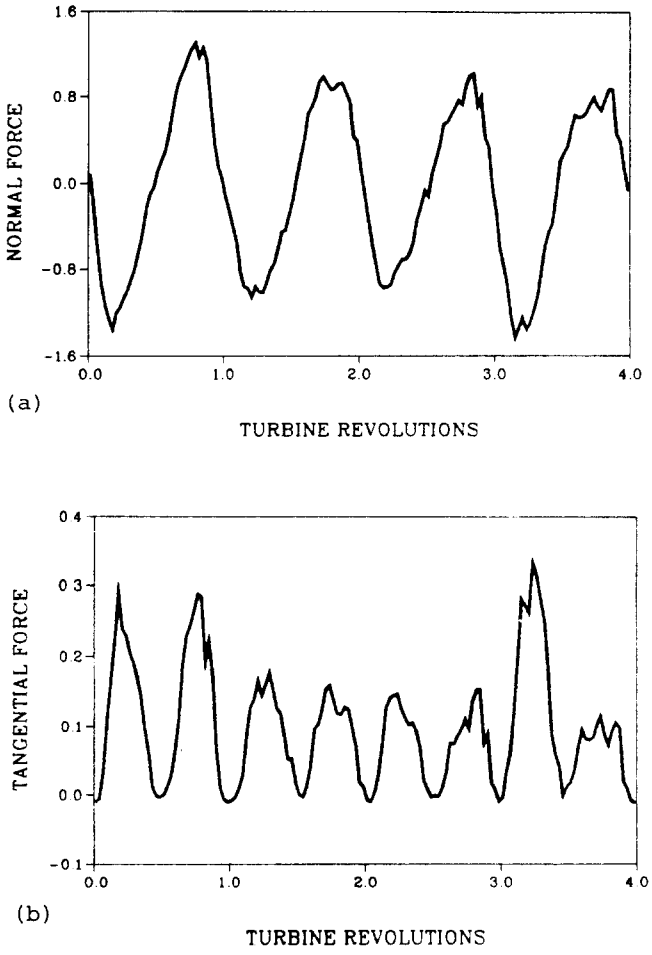

Fig. 8 Dimensionless Blade Loads calculated using a turbulent wind; (a) normal to the blade path, (b) tangent to the blade path.

Standard random data analysis can not be applied to this data until the deterministic part has been removed. Since the deterministic part can be represented by a sum of frequency components at the per rev frequencies, it can be removed by filtering those frequencies. The Buys-Ballot filter is perfectly suited to this purpose[12]. Fig. 9 contains psd's of the normal and tangential forces near the equator of a VAWT blade after the per rev frequency content has been extracted with the Buys-Ballot filter. The sharp downward spikes in the spectra of Fig. 9 indicate where the per rev components have been removed.

As may be seen by comparing Fig. 9 with Fig. 4, the low frequency content of the tangential forces is a quasi-static reflection of the energy present in the turbulence. The blade load psd's have much more high frequency content than would be expected by examining the turbulence psd. There are two reasons for this. First, the motion of the blade through the air causes the frequency content of the wind that the blade sees to shift to higher frequencies. This is much like the situation where the frequency content of the loads on a car traveling over a rough road depend on the speed of the car. The more energetic low frequencies of the wind are transformed into higher frequency loads. Second, relatively small changes in the incident wind at the blade can cause large changes in the induced angle of attack, and therefore large changes in the load. This magnifies the low energy, high frequency part of the turbulence spectrum.

Table 2 shows the dimensionless forces due to a turbulent wind which has been separated into deterministic and random parts by the Buys-Ballot filter. The deterministic part is written in terms of sine and cosine coefficients. The "%RANDOM" is the percentage of the total variance of the blade load in a one per rev band around each per rev frequency due to the random part. At low frequency, the random part is comparable to the deterministic per rev's, but it dominates the loads at the higher frequencies.

TABLE 2

PER REV FREQ.	NORMAL			TANGENTIAL		
	COS	SIN	%RANDOM	COS	SIN	%RANDOM
1	-2.24	18.7	17.	.029	-.891	69.
2	1.24	2.28	67.	-1.52	-.387	45.
3	.260	1.31	77.	-.101	.212	89.
4	.004	.225	98.	-.211	-.004	90.
5	-.084	.129	99.	-.019	.031	99.

Table 2 The frequency content of the blade loads, calculated using a turbulent wind ($\bar{V}$ = 21 mph), is divided into one per rev wide bands around each per rev frequency. The deterministic per rev frequencies are written in terms of cosine and sine coefficients. The random part is written as a percentage of the total variance in each frequency band.

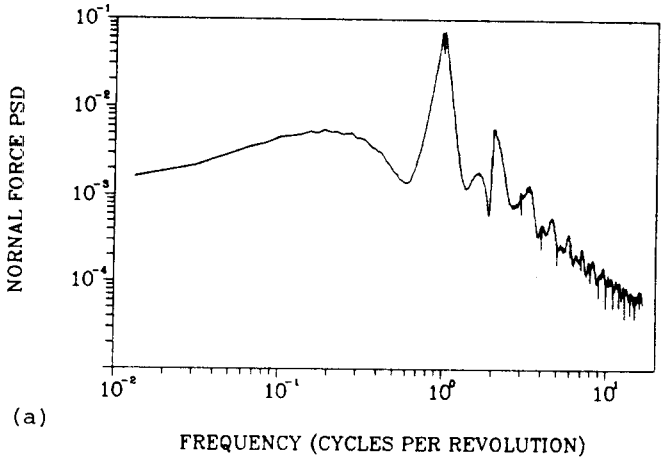

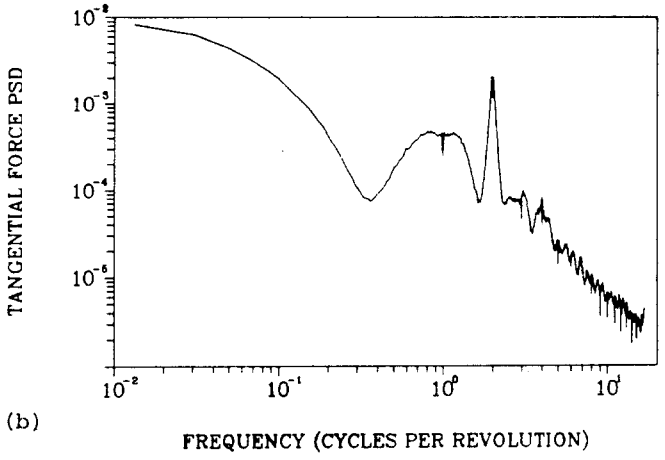

Fig. 9 Power spectral densities (psd's) of the blade loads calculated using a turbulent wind. The per rev frequency content has been removed so only the random part remains; (a) normal force psd, (b) tangential force psd.

An important difference between the steady and the turbulent wind loads is the change in the deterministic sine and cosine coefficients. As indicated by Tables 1 and 2, this difference is greatest for the tangential forces and at higher frequencies. If the relationship between wind and blade loads were linear, the coefficients would be identical in both cases. The fact that they are very close indicates that, for this example, where stall is not occurring ($\bar{V}$ = 21 mph), the nonlinearities are relatively small.

If a higher wind case is examined ($\bar{V}$ = 34 mph), the change in the per rev components is more dramatic. The sine and cosine coefficients for loads calculated assuming a steady wind which causes a significant amount of stall are shown in Table 3. The results from a turbulent wind with

TABLE 3

PER REV FREQ.	NORMAL		TANGENTIAL	
	COS	SIN	COS	SIN
1	-3.62	27.6	1.32	-.508
2	-1.90	8.82	-1.60	.818
3	.153	3.56	-2.17	-1.25
4	1.69	-1.24	-.931	-.391
5	.237	.508	-.569	1.03

Table 3 Cosine and sine coefficients of a Fourier series representation of the VAWT loads calculated assuming a steady wind. ($\bar{V}$ = 34 mph)

the same mean wind speed as above is shown in Table 4. The magnitudes of the components are approximate since the aerodynamic stall model is not exact. However, the trend in the data is apparent. Although the random part of the loads is not much different than it was for the case of low winds without stall (higher at some per revs and lower at others), the per rev components are noticeably lower for the turbulent wind case. For this mean wind speed, Table 5 shows the percentage difference in the rms deterministic loads for the two models. For high winds, the loads due to the steady mean wind are not the same as the mean loads due to a turbulent wind. Structural response calculations using the steady wind load estimates have had a tendency to match field data quite well at low wind speeds and deviate at higher wind speeds. Fig. 10 is a comparison of measured VAWT blade stress and estimated stress

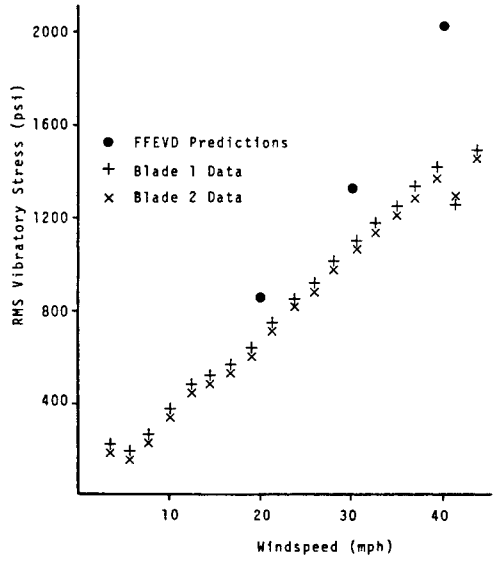

Fig. 10 Comparison of measured VAWT stress response and stresses calculated using steady wind loads. The analysis code is "FFEVD." Data were collected from both blades of the turbine.

response using steady wind input as reported by Lobitz and Sullivan[4]. The overprediction of the stress response in high winds is consistent with the overprediction of blade forces which results from assuming a steady wind.

The correlations and phase relationships between the loads at different points on the rotor are contained in the csd's. The complex csd can be expressed in terms of its magnitude and phase. The level of correlation is estimated using Eq. 5 by calculating the coherence function from the csd magnitude. The phase and coherence between identical points on opposite blades of a two bladed rotor are shown in Fig. 11. Fig. 12 shows the phase and coherence between loads on the same blade but separated by a distance of one fifth of the rotor height. Both Figs. 11 and 12 are for a 50ft (15m) diameter turbine using a one dimensional wind simulation at low wind speeds where there is no stall. The coherence function is a measure of the correlation of the calculated loads. The coherence is also useful as an estimate of the statistical significance of the calculated phase. A coherence near one indicates a consistent phase relationship between the loads at that frequency while a coherence near zero indicates that the calculated phase has no meaning. The coherence is generally low at high frequency and during changes in the phase. A high coherence is generaly found near per rev frequencies. However, high coherences tend to repeat at frequency intervals somewhat wider than one per rev. The cause of this effect is not clear, although it has been found independently by Anderson[13], using a frequency domain approach.

Larger diameter turbines were also examined with the one dimensional wind model. The only differences were an overall reduction in the coherence and a slight increase in the percent random contribution for the larger turbines. The psd's and phase relationships remained essentially the same. Another factor which increases the random contribution is the amount of atmospheric turbulence. This is controlled in the model by adjusting the surface roughness coefficient (z_o).

Summary and Conclusions

A method for simulating a single point wind time series is outlined. This method produces a Gaussian random process with the specified turbulence power spectral density. One dimensional variations are obtained by using Taylor's frozen turbulence hypothesis and a single point wind time

TABLE 4

PER REV FREQ.	NORMAL			TANGENTIAL		
	COS	SIN	%RANDOM	COS	SIN	%RANDOM
1	-3.40	27.1	10.	1.32	.202	76.
2	-1.43	8.35	50.	-1.36	-.607	73.
3	-.069	3.33	72.	-1.57	-.776	89.
4	.762	-.111	95.	-.936	-.348	81.
5	.248	.153	99.	.055	.246	97.

Table 4 The frequency content of the blade loads, calculated using a turbulent wind ($\bar{V}$ = 34 mph), is divided into one per rev wide bands around each per rev frequency. The deterministic per rev frequencies are written in terms of cosine and sine coefficients. The random part is written as a percentage of the total variance in each frequency band.

TABLE 5

PER REV FREQ.	NORMAL			TANGENTIAL		
	Steady	Turbulent	% diff.	Steady	Turbulent	% diff.
1	19.7	19.3	-2.0	1.00	.994	-5.6
2	6.38	5.99	-6.1	1.27	1.05	-17.3
3	2.52	2.36	-6.5	1.77	1.24	-30.0
4	1.48	.545	-63.2	.714	.706	-1.1
5	.396	.206	-48.0	.832	.178	-78.6

Table 5 The deterministic rms variation at each per rev frequency is shown for loads calculated in a 34 mph mean wind speed assuming both steady and turbulent winds. The percentage difference between them is also shown.

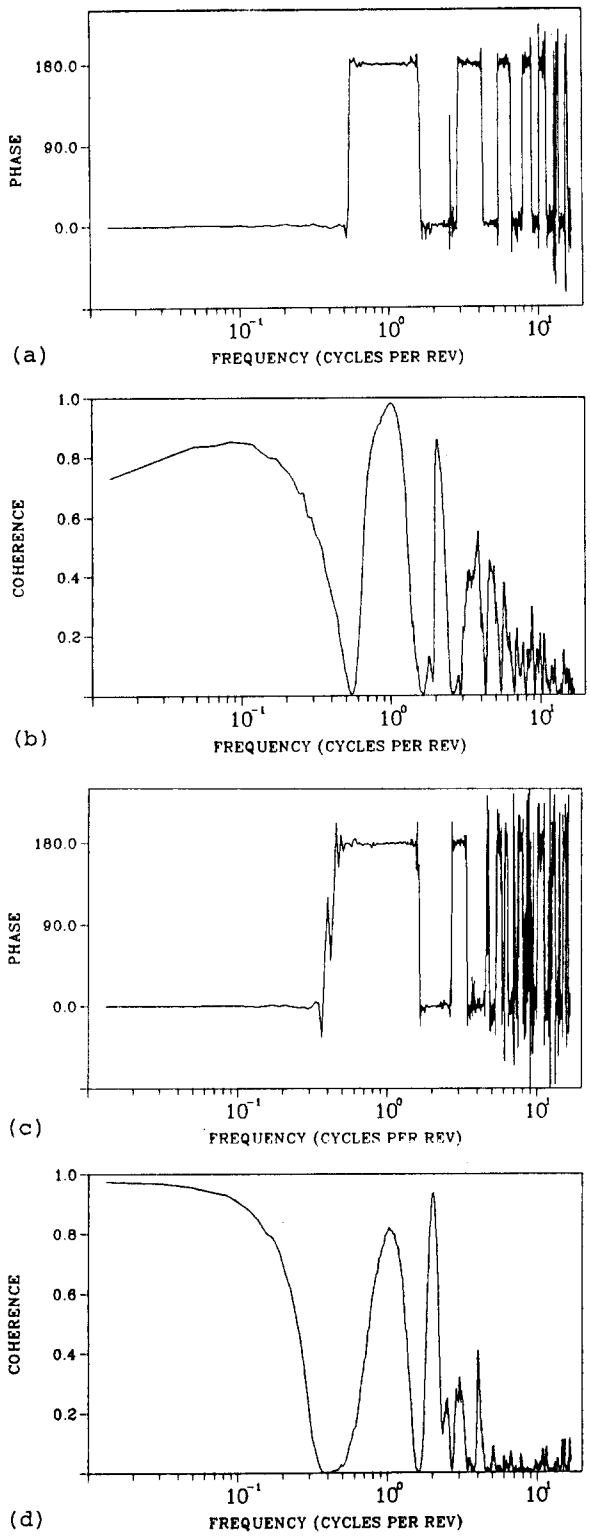

Fig. 11 Estimates of phase and coherence between the loads at the equator of the two blades of a VAWT rotor; (a) and (b) are for the normal forces, (c) and (d) are for the tangential forces.

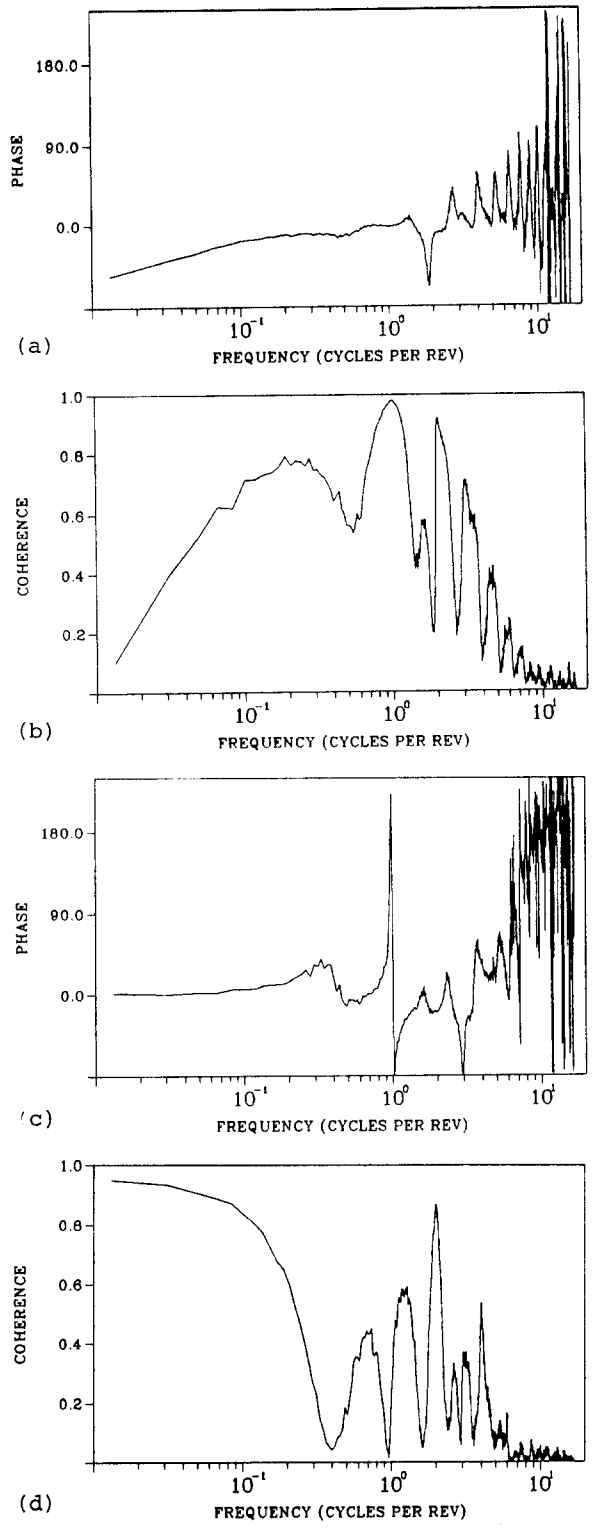

Fig. 12 Estimates of phase and coherence between the loads at two different points, separated by a distance of one fifth of the rotor height, on the same blade; (a) and (b) are for the normal forces, (c) and (d) are for the tangential forces.

series. A three dimensional wind simulation is produced by creating single point simulations at a number of input points. These time series are random and partially correlated in a way that matches the empirical coherence function suggested by Frost.

The simulated wind turbulence is tracked as it passes through the rotor by using a multiple streamtube representation of the flow. Blade loads are calculated using a momentum balance approach developed by Strickland. Before reducing the blade load time series to the form of psd's and csd's, the random and deterministic parts are separated using the Buys-Ballot filter.

The load psd's indicate that the turbulent energy in the wind is shifted to higher frequencies in the blade loads. This is due both to the motion of the blade through the turbulence and the magnifying effect of small variations in angle of attack. The percentage of the total variance of the load that is random is comparable to the per rev contribution at lower frequency, but it dominates the loads at higher frequency. This random percentage increases with turbine size and amount of turbulence.

The most important result is that when steady winds are assumed, the high wind per rev loads are overpredicted. This is consistent with the difference between actual measured stresses and stresses calculated using the steady wind model. The difference between the deterministic per rev components in steady and turbulent winds is due to the nonlinearity in the relationship between angle of attack and blade load, especially in high winds where stall in occurring. The actual magnitude of the difference has not been determined since the aerodynamic stall model is approximate. More accurate estimates of the stochastic loads in high winds require a validated dynamic stall model.

References

1. Templin, R. J., "Aerodynamic Performance Theory for the NRC Vertical-Axis Wind Turbine," National Research Council of Canada Report LTR-LA-160, June, 1974.

2. Strickland, J. H., Smith, T., and Sun, K., "A Vortex Model of the Darrieus Turbine: An Analytical and Experimental Study," SAND81-7017 (Albuquerque, NM: Sandia National Laboratories, June, 1981).

3. Carne, T. G., Lobitz, D. W., Nord, A. R., Watson, R. A., "Finite Element Analysis and Modal Testing of a Rotating Wind Turbine," SAND82-0345 (Albuquerque, NM: Sandia National Laboratories, October, 1982).

4. Lobitz, D. W., and Sullivan, W. N., "A Comparison of Finite Element Predictions and Experimental Data for the Forced Response of the DOE 100kW Vertical Axis Wind Turbine," SAND82-2584 (Albuquerque, NM: Sandia National Laboratories, February, 1984).

5. Frost, Walter, Long, D. H., and Turner, R. E., "Engineering Handbook on the Atmospheric Environment Guideline for Use in Wind Turbine Generator Development," NASA Technical Paper 1359, December, 1979.

6. Shinozuka, M., "Simulation of Multivariate and Multidimensional Random Processes," Journal of the Acoustical Society of America, Vol. 49, No. 1 (part 2), p. 357, 1971.

7. Smallwood, D. O., "Random Vibration Testing of a Single Test Item with a Multiple Input Control System," Proceedings of the Institute of Environmental Sciences, April, 1982.

8. Thresher, R. W., Holley, W. E., Smith, C. E., Jafarey, N., Lin, S.-R., "Modeling the Reponse of Wind Turbines to Atmospheric Turbulence," U. S. Department of Energy Report DOE/ET/23144-81/2, August, 1981.

9. Thresher, R. W., Holley, W. E., Hershberg, E. L., Lin, S.-R., "Response of the MOD-0A Wind Turbine Rotor to Turbulent Atomospheric Winds," U. S. Department of Energy Report DOE/RL/10378-82/1, October, 1983.

10. Fichtl, G. H., "Covariance Statistics of Turbulence Velocity Components for Wind Energy Conversion System Design - Homogeneous, Isotropic Case," PNL-3499 (Pacific Northwest Laboratories, Richland, WA), September, 1983.

11. Strickland, J. H., "The Darrieus Turbine: A Performance Prediction Model Using Multiple Streamtubes," SAND75-0431 (Albuquerque, NM: Sandia National Laboratories, October, 1975).

12. Koopmans, L. H., The Spectral Analysis of Time Series, Academic press, New York, 1974.

13. Anderson, M. B., Sir Robert McAlpine & Sons, Ltd., London, UK, private correspondence, May, 1984.

DISTRIBUTION:

Aerolite, Inc.
550 Russells Mills Road
South Dartmouth, MA 02748
Attn: R. K. St. Aubin

Alcoa Technical Center (4)
Aluminum Company of America
Alcoa Center, PA 15069
Attn: D. K. Ai
J. T. Huang
J. R. Jombock
J. L. Prohaska

Alternative Sources of Energy
Milaca, MN 56353
Attn: Larry Stoiaken

Amarillo College
Amarillo, TX 79100
Attn: E. Gilmore

American Wind Energy Association
1516 King Street
Alexandria, VA 22314

Arizona State University
University Library
Tempe, AZ 85281
Attn: M. E. Beecher

Atlantic Wind Test Site
P.O. Box 189
Tignish P.E.I.
CANADA COB 2BO
Attn: R. G. Richards

Battelle-Pacific Northwest Laboratory (4)
P. O. Box 999
Richland, WA 99352
Attn: J. R. Connell
R. L. George
D. C. Powell
L. Wendell

Dr. George Bergeles
Dept. of Mechanical Engineering
National Technical University
42, Patission Street
Athens, GREECE

Bonneville Power Administration
P.O. Box 3621
Portland, OR 97225
Attn: N. Butler

Burns & Roe, Inc.
800 Kinderkamack Road
Oradell, NJ 07649
Attn: G. A. Fontana

California State Energy Commission
Research and Development Division
1111 Howe Avenue
Sacramento, CA 95825
Attn: J. Lerner

Canadian Standards Association
178 Rexdale Blvd.
Rexdale, Ontario
CANADA M9W 1R3
Attn: Tom Watson

Professor V. A. L. Chasteau
School of Engineering
University of Auckland
Private Bag
Auckland, NEW ZEALAND

Colorado State University
Dept. of Civil Engineering
Fort Collins, CO 80521
Attn: R. N. Meroney

Commonwealth Electric Co.
Box 368
Vineyard Haven, MA 02568
Attn: D. W. Dunham

Gale B. Curtis
Curtis Associates
3089 Oro Blanco Drive
Colorado Springs, CO 80917

M. M. Curvin
11169 Loop Road
Soddy Daisy, TN 37379

Department of Economic Planning
and Development
Barrett Building
Cheyenne, WY 82002
Attn: G. N. Monsson

Otto de Vries
National Aerospace Laboratory
Anthony Fokkerweg 2
Amsterdam 1017
THE NETHERLANDS

DOE/ALO
Albuquerque, NM 87115
Attn: G. P. Tennyson

DOE/ALO
Energy Technology Liaison Office
NGD
Albuquerque, NM 87115
Attn: Capt. J. L. Hanson, USAF

DOE Headquarters (20)
Wind Energy Technology Division
1000 Independence Avenue
Washington, DC 20585
Attn: L. V. Divone
P. Goldman

Dominion Aluminum Fabricating, Ltd. (2)
3570 Hawkestone Road
Mississauga, Ontario
CANADA L5C 2V8
Attn: D. Malcolm
L. Schienbein

J. B. Dragt
Nederlands Energy Research Foundation (E.C.N.)
Physics Department
Westerduinweg 3 Patten (nh)
THE NETHERLANDS

Dynergy Systems Corporation
821 West L Street
Los Banos, CA 93635
Attn: C. Fagundes

Electric Power Research Institute (3)
3412 Hillview Avenue
Palo Alto, CA 94304
Attn: E. Demeo
F. Goodman
S. Kohan

Dr. Norman E. Farb
10705 Providence Drive
Villa Park, CA 92667

Alcir de Faro Orlando
Pontificia Universidade Catolica-PUC/Rj
Mechanical Engineering Department
R. Marques de S. Vicente 225
Rio de Janeiro, BRAZIL

FloWind Corporation (4)
21414 68th Avenue South
Kent, WA 98031
Attn: Herman M. Drees
S. Tremoulet
I. E. Vas
R. Watson

Gates Learjet
Mid-Continent Airport
P.O. Box 7707
Wichita, KS 67277
Attn: G. D. Park

H. Gerardin
Mechanical Engineering Department
Faculty of Sciences and Engineering
Universite Laval-Quebec
CANADA G1K 7P4

R. T. Griffiths
University College of Swansea
Dept. of Mechanical Engineering
Singleton Park
Swansea SA2 8PP
UNITED KINGDOM

Helion, Inc.
Box 445
Brownsville, CA 95919
Attn: Jack Park, President

Institut de recherche d'Hydro-Quebec (3)
1800, Montee Ste-Julie
Varennes, Quebec
Canada JOL 2PO
Attn: Gaston Beaulieu
Bernard Masse
Ion Paraschivoiu

Iowa State University
Agricultural Engineering, Room 213
Ames, IA 50010
Attn: L. H. Soderholm

JBF Scientifcic Corporation
2 Jewel Drive
Wilmington, MA 01887
Attn: E. E. Johanson

Kaiser Aluminum and Chemical Sales, Inc.
14200 Cottage Grove Avenue
Dolton, IL 60419
Attn: A. A. Hagman

Kaiser Aluminum and Chemical Sales, Inc.
6177 Sunol Blvd.
P.O. Box 877
Pleasonton, CA 94566
Attn: D. D. Doerr

Kaman Aerospace Corporation
Old Windsor Road
Bloomfield, CT 06002
Attn: W. Batesol

Kansas State University
Electrical Engineering Department
Manhattan, KS 66506
Attn: Dr. G. L. Johnson

R. E. Kelland
The College of Trades and Technology
P.O. Box 1693
Prince Philip Drive
St. John's, Newfoundland
CANADA A1C 5P7

KW Control Systems, Inc.
RD#4, Box 914C
South Plank Road
Middletown, NY 10940
Attn: R. H. Klein

Kalman Nagy Lehoczky
Cort Adelers GT. 30
Oslo 2
NORWAY

L. Liljidahl
Building 005, Room 304
Barc-West
Beltsville, MD 20705

Olle Ljungstrom
FFA, The Aeronautical Research Institute
Box 11021
S-16111 Bromma
SWEDEN

Massachusetts Institute of Technology (2)
77 Massachusetts Avenue
Cambridge, MA 02139
Attn: Professor N. D. Ham
W. L. Harris, Aero/Astro Dept.

H. S. Matsuda
Composite Materials Laboratory
Pioneering R&D Laboratories
Toray Industries, Inc.
Sonoyama, Otsu, Shiga
JAPAN 520

Michigan State University
Division of Engineering Research
East Lansing, MI 48825
Attn: O. Krauss

Napier College of Commerce and Technology
Tutor Librarian, Technology Faculty
Colinton Road
Edinburgh, EH10 5DT
ENGLAND

NASA Lewis Research Center (2)
21000 Brookpark Road
Cleveland, OH 44135
Attn: D. Baldwin
J. Savino

National Rural Electric Cooperative Assn
1800 Massachusetts Avenue NW
Washington, DC 20036
Attn: Wilson Prichett III

Natural Power, Inc.
New Boston, NH 03070
Attn: Leander Nichols

Northwestern University
Dept. of Civil Engineering
Evanston, IL 60201
Attn: R. A. Parmalee

Ohio State University
Aeronautical and Astronautical Dept.
2070 Neil Avenue
Columbus, OH 43210
Attn: Professor G. Gregorek

Oklahoma State University
Mechanical Engineering Dept.
Stillwater, OK 76074
Attn: D. K. McLaughlin

Oregon State University (2)
Mechanical Engineering Dept.
Corvallis, OR 97331
Attn: W. E. Holley
R. E. Wilson

Pacific Gas & Electric
3400 Crow Canyon Road
San Ramon, CA 94583
Attn: T. Hillesland

Troels Friis Pedersen
Riso National Laboratory
Postbox 49
DK-4000 Roskilde
DENMARK

Helge Petersen
Riso National Laboratory
DK-4000 Roskilde
DENMARK

The Power Company, Inc.
P.O. Box 221
Genesee Depot, WI 53217
Attn: A. A. Nedd

Public Service Co. of New Hampshire
1000 Elm Street
Manchester, NH 03105
Attn: D. L. C. Frederick

Public Service Company of New Mexico
P.O. Box 2267
Albuquerque, NM 87103
Attn: M. Lechner

RANN, Inc.
260 Sheridan Ave., Suite 414
Palo Alto, CA 94306
Attn:Alfred J. Eggers, Jr.
Chairman of the Board

Renewable Energy Ventures
190 South King Street, Suite 2460
Honolulu, HI 96813
Attn: G. W. Stricker

The Resources Agency
Department of Water Resources
Energy Division
1416 9th Street
P.O. Box 388
Sacramento, CA 95802
Attn: R. G. Ferreira

Reynolds Metals Company
Mill Products Division
6601 West Broad Street
Richmond, VA 23261
Attn: G. E. Lennox

A. Robb
Memorial University of Newfoundland
Faculty of Engineering and Applied Sciences
St. John's Newfoundland
CANADA A1C 5S7

Rockwell International (2)
Rocky Flats Plant
P.O. Box 464
Golden, CO 80401
Attn: Terry Healy

Dr. -Ing. Hans Ruscheweyh
Institut fur Leichbau
Technische Hochschule Aachen
Wullnerstrasse 7
GERMANY

Beatrice de Saint Louvent
Establissement d'Etudes et de Recherches
Meteorologigues
77, Rue de Serves
92106 Boulogne-Billancourt Cedex
FRANCE

Gwen Schreiner
Librarian
National Atomic Museum
Albuquerque, NM 87185

Arnan Seginer
Professor of Aerodynamics
Technion-Israel Institute of Technology
Department of Aeronautical Engineering
Haifa, ISRAEL

David Sharpe
Kingston Polytecnic
Canbury Park Road
Kingston, Surrey
UNITED KINGDOM

Kent Smith
Instituto Technologico Costa Rico
Apartado 159 Cartago
COSTA RICA

Solar Initiative
Citicorp Plaza, Suite 900
180 Grand Avenue
Oakland, CA 94612
Attn: Jerry Yudelson

Bent Sorenson
Roskilde University Center
Energy Group, Bldg. 17.2
IMFUFA
P.O. Box 260
DK-400 Roskilde
DENMARK

South Dakota School of Mines and Technology
Dept. of Mechanical Engineering
Rapid City, SD 57701
Attn: E. E. Anderson

Southern California Edison
Research & Development Dept., Room 497
P.O. Box 800
Rosemead, CA 91770
Attn: R. L. Scheffler

Southern Illinois University
School of Engineering
Carbondale, IL 62901
Attn: C. W. Dodd

G. Stacey
The University of Reading
Department of Engineering
Whiteknights, Reading, RG6 2AY
ENGLAND

Stanford University
Mechanical Engineering,
Design Division
Stanford, CA 94305
Attn: Drew Nelson

Stanford University (2)
Civil Engineering Department
Stanford, CA 94305
Attn: C. A. Cornell
S. Winterstien

Stanford University
Dept. of Aeronautics and
Astronautics Mechanical Engineering
Stanford, CA 94305
Attn: Holt Ashley

R. J. Templin (3)
Low Speed Aerodynamics Laboratory
NRC-National Aeronautical Establishment
Montreal Road
Ottawa, Ontario, K1A 0R6
CANADA

Texas Tech University (2)
Mechanical Engineering Dept.
P.O. Box 4389
Lubbock, TX 79409
Attn: J. W. Oler
J. Strickland

Tulane University
Dept. of Mechanical Engineering
New Orleans, LA 70018
Attn: R. G. Watts

Tumac Industries, Inc.
650 Ford Street
Colorado Springs, CO 80915
Attn: J. R. McConnell

J. M. Turner
Terrestrial Energy Technology Program Office
Energy Conversion Branch
Aerospace Power Division
Aero Propulsion Laboratory
Air Force Wright Aeronautical Laboratories
Wright-Patterson Air Force Base, OH 45433

United Engineers and Constructors, Inc.
PO Box 8223
Philadelphia, PA 19101
Attn: A. J. Karalis

University of Alaska
Geophysical Institute
Fairbanks, AK 99701
Attn: T. Wentink, Jr.

University of California
Institute of Geophysics
and Planetary Physics
Riverside, CA 92521
Attn: Dr. P. J. Baum

University of Colorado
Dept. of Aerospace Engineering Sciences
Boulder, CO 80309
Attn: J. D. Fock, Jr.

University of Massachusetts
Mechanical and Aerospace Engineering Dept.
Amherst, MA 01003
Attn: Dr. D. E. Cromack

University of New Mexico
New Mexico Engineering Research Institute
Campus P.O. Box 25
Albuquerque, NM 87131
Attn: G. G. Leigh

University of Oklahoma
Aero Engineering Department
Norman, OK 73069
Attn: K. Bergey

University of Sherbrooke
Faculty of Applied Science
Sherbrooke, Quebec
CANADA J1K 2R1
Attn: R. Camerero

The University of Tennessee
Dept. of Electrical Engineering
Knoxville, TN 37916
Attn: T. W. Reddoch

USDA, Agricultural Research Service
Southwest Great Plains Research Center
Bushland, TX 79012
Attn: Dr. R. N. Clark

Utah Power and Light Co.
51 East Main Street
P.O. Box 277
American Fork, UT 84003
Attn: K. R. Rasmussen

VAWTPOWER, Inc.
9733 Coors NW
Albuquerque, NM 87114
Attn: P. N. Vosburgh

Washington State University
Dept. of Electrical Engineering
Pullman, WA 99163
Attn: F. K. Bechtel

West Texas State University
Government Depository Library
Number 613
Canyon, TX 79015

West Texas State University
Department of Physics
P.O. Box 248
Canyon, TX 79016
Attn: V. Nelson

West Virginia University
Dept. of Aero Engineering
1062 Kountz Avenue
Morgantown, WV 26505
Attn: R. Walters

D. Westlind
Central Lincoln People's Utility District
2129 North Coast Highway
Newport, OR 97365-1795

Wichita State University
Aero Engineering Department (2)
Wichita, KS 67208
Attn: M. Snyder
W. Wentz

Wind Energy Report
Box 14
102 S. Village Avenue
Rockville Centre, NY 11571
Attn: Farrell Smith Seiler

Wind Power Digest
P. O. Box 700
Bascom, OH 44809
Attn: Michael Evans

Wisconsin Division of State Energy
8th Floor
101 South Webster Street
Madison, WI 53702
Attn: Wind Program Manager

Robert Akins
Professor of Engineering
Washington and Lee University
Lexington, VA 24450

Dr. Michael B. Anderson
Sir Robert McAlpine & Sons, Ltd.
P. O. Box 74
40 Bernard Street
London WC1N 1LG
ENGLAND

Theodore S. Anderson
Advanced Energy Systems Division
Westinghouse Electric Corporation
P. O. Box 10864
Pittsburgh, PA 15236

1520	D. J. McCloskey
1522	R. C. Reuter, Jr.
1523	J. H. Biffle
1523	D. B. Clauss
1524	D. W. Lobitz
1524	P. S. Veers (25)
1524	W. N. Sullivan
1600	R. G. Clem
1630	R. C. Maydew
1633	R. E. Sheldahl
1636	J. K. Cole
2525	R. P. Clark
3141-1	C. M. Ostrander
3151	W. L. Garner (3)
3154-3	C. H. Dalin (28) for DOE/TIC (Unlimited Release)
3160	J. E. Mitchell (15)
3161	P. S. Wilson
6000	E. H. Beckner
6200	V. L. Dugan
6220	D. G. Schueler
6225	R. H. Braasch (50)
6225	D. E. Berg
6225	J. D. Cyrus
6225	R. D. Grover
6225	E. G. Kadlec
6225	P. C. Klimas
6225	M. T. Mattison
6225	R. O. Nellums
6225	D. S. Oscar
6225	M. H. Worstell
7111	J. W. Reed
7543	R. Rodeman
8024	M. A. Pound